Differential impact of isolated topographic bumps on glacial ice flow and subglacial processes

Marion A. McKenzie[1], Lauren M. Simkins[1], Jacob S. Slawson[1*], Emma J. MacKie[2], and Shujie Wang[3]

[1]Department of Environmental Sciences, University of Virginia, 291 McCormick Rd., Charlottesville, VA 22904
[2]Department of Geological Sciences, University of Florida, 241 Williamson Hall, Gainesville, PL 32611-2120
[3]Department of Geography, Pennsylvania State University, 302 N Burrowes St., University Park, PA 16802
*Current affiliation: Department of geology and Geological Engineering, Colorado School of Mines, 1516 Illinois St., Golden, CO 80401

Correspondence to: Marion A. McKenzie (mm8dt@virginia.edu)

Abstract. Topographic highs ("bumps") across glaciated landscapes have the potential to temporarily slow glacial ice flow or, conversely, increase ice flow through strain heating and subglacial meltwater production. Isolated bumps of variable size across the deglaciated landscape of the Cordilleran Ice Sheet (CIS) of Washington state present an opportunity to assess the influence of topographic highs on ice-bed interactions and ice flow organization. This work utilizes semi-automatic mapping techniques of subglacial bedforms to characterize the morphology of streamlined subglacial bedforms including elongation, surface relief, and orientation -- all of which provide insight into subglacial processes during post-Last Glacial Maximum deglaciation of the landscape. We identify a bump-size threshold of ~ 4.5 km^3 in which bumps larger than this size will consistently and significantly disrupt both ice-flow organization and subglacial sedimentary processes -- fundamental to the genesis of streamlined subglacial bedforms. Additionally, sedimentary processes are most mature downstream of bumps as reflected by enhanced bedform elongation and reduced surface relief, likely due to increased availability and production of subglacial sediment and meltwater. While isolated topography is found to play a role in disrupting ice flow, not all bumps have the same degree of impact. The variable influence of isolated topographic bumps on ice flow in this system has significance for outlet glaciers of the Greenland Ice Sheet (GrIS) due to general topographic similarities.

1 Introduction

Isolated topographic highs in the terrain beneath ice sheets can contribute to increased basal drag and decreased ice flow velocity and, for marine-based margins, offer pinning-points to halt or slow down margin retreat (Durand et al., 2011; Favier et al., 2016; Alley et al., 2021; Robel et al., 2022). Conversely, ice flow over topographic highs can increase strain heating and basal meltwater production, elevating basal meltwater pressure and reducing basal friction in the downstream environment

(Payne and Dongelmans, 1997; Cuffey and Paterson, 2010). However, identifying which forms and scales of “bumps” across a glaciated landscape may increase, decrease, or not affect ice-flow velocity, basal water pressure, and basal friction is not well understood. Additionally, basal topography at the base of the ice sheet – and even for most glacier catchments – is poorly resolved (e.g., MacKie et al., 2020; Morlighem et al., 2020). Therefore, we turn to a formerly glaciated landscape in Washington state where geomorphological indicators of ice-flow conditions in the form of streamlined subglacial bedforms, such as glacial lineations, whalebacks, and drumlins, can be used to better understand the sensitivity of ice sheets to isolated bumps in the subglacial environment. Morphometrics of streamlined subglacial bedforms offer information on ice-bed interactions and provide an opportunity to assess characteristics of paleo-ice flow organization and relative speeds across a landscape (e.g., Clark, 1997, 1999; King et al., 2009; Clark et al., 2003, 2009; Spagnolo et al., 2012, 2014; Principato et al., 2016). Assessment of streamlined subglacial bedforms and their implications for ice flow are applicable to modern ice sheets (MacKie et al., 2021), where empirical observations of subglacial conditions are spatially (and temporally) limited.

1.1 Site Characteristics

The Puget Lowland of Washington state was glaciated by the southwestern Cordilleran Ice Sheet (CIS) during the Last Glacial Maximum (LGM), when the region was largely depressed below sea level due to glacial isostatic adjustment (GIA; Booth and Hallet, 1993; Dethier et al., 1995; Kovanen and Slaymaker, 2004; Eyles et al., 2018); therefore, the southwestern CIS was predominantly marine based. Active tectonics and volcanic activity across the Puget Lowland have led to exposed crystalline and volcanic bedrock of Eocene age interrupting sedimentary bedrock across the region (Khazaradze et al., 1999; Booth et al., 2004). Based on subglacial modeling (Alley et al., 2021), it is highly possible the higher relief crystalline and volcanic bedrock exposures or “bumps” influenced marine and terrestrial-based ice-bed interactions across the Puget Lowland, but this concept has yet to be empirically tested across the region. The Puget Lowland is a basin surrounded by mountainous terrain near the coast of the Pacific Ocean with isolated topographic highs, similar to the terrain beneath the margins of the Greenland Ice Sheet (Bamber et al. 2013; Eyles et al., 2018). This work aims to determine the role of topographic bumps on glacial ice flow via streamlined subglacial bedform morphology and distribution. By assessing ice flow behavior within a single glacial system, effects of isolated crystalline bedrock highs on ice flow will not be confounded by geographically variable conditions such as local climate and ocean forcings.

2. Methodology

2.1 Topographic “Bump” Classification

Digital elevation models with horizontal resolution of 1.83 x 1.83 meters and coarsest vertical resolution of 2 meters from across the Puget Lowland (Clallam County, Olympic Department of Natural Resources, WA, 2008; Quantum Spatial Inc., 2017, 2019; OCM Partners, 2019a, 2019b) and ambient occlusion hillshading techniques (c.f., McKenzie et al., 2022) were utilized to assess nine crystalline and volcanic bedrock bumps across the Puget Lowland with a wide range in peak elevation, bump surface area and volume, and topographic setting (Fig. 1). The outermost 100-foot closed contour across each bump was expanded to three times the surface area to classify the region of interest, following the influence of bump perturbations on basal hydrologic potential by Alley et al., 2021. While present-day elevations of these deglaciated sites differ from elevations during glaciation due to GIA, tectonics, and post-glacial landscape evolution, relative relief and influence of these bumps on the presence of streamlined bedforms is well preserved. Fractures, faults, and joints from tectonic activity and brittle deformation of the crust across bumps are below the scale of analysis for this work and are therefore not considered here.

2.2 Streamlined subglacial bedform identification

Streamlined subglacial bedforms were identified across the nine bump sites using a combination of Topographic Position Index (TPI) analysis (McKenzie et al., 2022), contour-tree mapping (Wang et al., 2017), and manual identification. TPI utilizes DEM slope variations across defined cell-neighborhood sizes to semi-automatically identify positive relief features (McKenzie et al., 2022). Localized contour-tree mapping utilizes DEM data to isolate closed contours within a defined elevation (Wang et al., 2017). Both tool outputs were validated and corrected if needed by manual removal of incorrectly identified features and manual addition of bedforms missed by the automated tools. All bedforms in the final dataset (n=3,273) have an associated long-axis length, cardinal orientation, width orthogonal to long-axis length, and range in elevation across the long axis calculated by the ArcGIS Pro “Minimum Bounding Geometry” and “Add Z Information” tools (McKenzie et al., 2023). For each site, bedforms were categorized into groups “upstream”, “on top of”, and “downstream” as determined by bedform location with respect to the outermost 100-foot contour of the topographic high. Bedforms identified “downstream” of bumps include bump-lateral features. Long axis cardinal direction, or orientation, of streamlined bedforms is used to infer direction of ice flow (Clark, 1997; Kleman et al., 2006; Kleman and Borgström, 1996). Bedform elongation ratio, calculated by dividing a bedform’s length by its width is used to infer relative speed of ice flow velocity (Clark 1997, 1999; Clark et al., 2003) and relative duration of ice presence in a region (Benediktsson et al., 2016). Bedform surface relief, the difference between the highest and lowest elevation along the bedform long axis, is used to infer maturity of ice flow and sedimentary processes in the subglacial environment, where smaller surface relief values indicate more mature sedimentary processes in the subglacial environment than larger values (McKenzie et al., 2022). We performed analysis of variance (ANOVA) and non-parametric Kruskal-Wallis tests to compare the statistical significance of the means and distributions between populations, respectively, in “R”. Results of statistical analyses were used to determine significance of bedform characteristics at each site (i.e., upstream, on top of, and downstream of bumps) as well as significance of bedform morphometrics across sites.

3. Results and Discussion

The number of streamlined bedforms per site is positively correlated with site surface area and volume (Fig. 1B), indicating spatial continuity in the bedform distribution across the Puget Lowland. On top of all bump sites, bedform elongation for the full dataset (n = 3,273) is lowest and bedform surface relief is highest (Fig. 2). We, thus, interpret that bumps in the subglacial environment of the Cordilleran Ice Sheet generally led to ice-flow deceleration and reduction of efficiency or spatial homogeneity of sedimentary processes including bedrock erosion and sediment transport and deposition – all of which are important for bedform genesis (Schoof and Clark, 2008; Shaw et al., 2008; King et al., 2009). While bedform surface relief and elongation ranges overlap across all site populations, bedforms associated with smaller bumps tend to have outliers below the 1σ (68%) confidence level for all populations (e.g., San Juan Island, Fidalgo Island, and Black Hills) while those associated with larger bumps have outliers above the 1σ confidence level (e.g., Blue Hills and Cougar Mountain; Fig. 2). This trend in outliers demonstrates a linkage between bump size and possible bedform morphometrics in a relatively systemic manner across the Puget Lowland. Notably, there is a significant decrease in bedform elongation between upstream and on top of the two largest bumps (Fig. 3A), Blue Hills and Devils Mountain, suggesting bump volume larger than 4.5 km^3 significantly slows or causes disorganization in ice flow (Fig. 1B; Clark 1997, 1999; Clark et al., 2003).

At seven of the nine sites, surface relief along bedform crests increases significantly between populations upstream and on top of bumps (Fig. 3B), most likely due to a transition in subglacial lithology from sedimentary to crystalline or volcanic bedrock, disrupting sedimentary processes as ice contacted more-erosion-resistant bed compositions. The two exceptions to this trend are Big Skidder Hill and Lopez Island, where there is no appreciable change in streamlined subglacial bedform surface relief across the bumps (Fig. 3B); therefore, suggesting that conditions at these two sites were able to overcome direct lithologic impact on bedform relief. Due to the more-erosion-resistant lithologies of the bumps, combined with increased pressure and basal drag in the subglacial environment, there is decreased efficiency in which the ice is able to facilitate streamlined subglacial bedform formation through bedrock erosion (Eyles and Doughty, 2016; Krabbendam et al., 2016), leading to truncated bedforms with high surface relief (McKenzie et al., 2022; Fig. 2). We postulate that bump size – through its impact on ice flow and subglacial processes – is a major control on bedform surface relief, where the greatest proportion of bedforms with low surface relief (Fig. 4B) are located at the smallest bump sites (< 0.2 km^3). Increased sediment availability and basal meltwater that results from the strain heating on top of the bump (Payne and Dongelmans, 1997), increases downstream sediment transport efficiency (McIntyre, 1985; Pohjola and Hedfors, 2003; Winsborrow et al., 2010b), resulting in the greatest number and most elongate bedforms, as well as the greatest proportion of bedforms with low surface relief, downstream of bumps (Fig. 1A; Fig. 2; Fig. 4A, 4B).

While many sites showcase an increase in disorganization of bedform orientation on top of the bump, only at the two largest bumps (> 4.5 km^3) does downstream bedform orientation recover to patterns present in the upstream bedform populations (Fig. 4C). The rest of the sites have bedform orientations that either remain unchanged or become more disorganized downstream (Fig. 4C). From these findings, we infer a bump volume of ~ 4.5 km^3 will influence reorganization of downstream ice-flow orientation and subglacial sedimentary processes, while bumps below this threshold cannot regain the same organization seen upstream of bumps. This analysis found no evidence of channelized meltwater in the subglacial environment, potentially suggesting meltwater development across these bumps was distributed and saturated, which would explain the homogeneity in bedform formation observed in bedforms downstream of bumps.

4. Conclusions

Overall, there is general ice flow deceleration and reduction of bedrock erosion efficiency on top of bumps, which results from a subglacial lithology transition. Sedimentary processes, essential to streamlined bedform genesis, are most organized and efficient downstream of bumps - likely as a result of increased sediment availability and subglacial meltwater sourced from strain heating on top of the bump. The largest sites notably disturb ice-flow orientation and speed on top of the bump with only bumps larger than ~4.5 km^3 indicating recovery of ice flow orientation and speed downstream of bumps. Findings from these paleo-subglacial bumps may be used as an analog for ice flow in contemporary ice sheets and support process-based understanding of subglacial terrain influence on overlying ice-sheet behavior in similar systems.

5. Data availability

All bedform data produced from this work is publicly available through PANGAEA and are available by request from the corresponding author.

6. Author contribution

Project conceptualization, data curation, methodology, formal analysis, initial draft writing, and editing were conducted by M. McKenzie. Conceptualization, funding acquisition, formal analysis, editing, and supervision were conducted by L. Simkins. Conceptualization, preliminary research, and editing were conducted by J. Slawson. Partial conceptualization and editing were conducted by E. MacKie. Support with data curation and editing were conducted by S. Wang.

7. Competing interests

The authors declare that they have no conflict of interest.

8. Acknowledgments

We acknowledge the Washington Department of Natural Resources for their accessible LiDAR data that made this project possible. The sites analyzed for this work are located on land historically cultivated and inhabited by the Skokomish, Suquamish, Squaxin, Stl'pulmsh, Steilacoom, Puyallup, Muckleshoot, and Duwamish peoples, while much of the data analysis and interpretation were conducted on land cultivated and inhabited by the Monacan Nation. The peoples of these Nations were custodians of the land for time immemorial before forced removal and genocide during colonization. The authors acknowledge their ongoing stewardship of the lands. This work was funded by the Chamberlain Endowment and the H.G. Goodell Endowment at the University of Virginia.

References

Alley, R.B., Holschuh, N., MacAyeal, D.R., Parizek, B.R., Zoet, L., Riverman, K., Muto, A., Christianson, K., Clyne, E., Anandakrishnan, S., Stevens, N., GHOST Collaboration: Bedforms of Thwaites Glacier, West Antarctica: Character and Origin, Journal of Geophysical Research: Earth Surface, 126:12. https://doi.org/10.1029/2021JF006339, 2021.

Bamber, J.L., Griggs, J.A., Hurkmans, R.T.W.L., Dowdeswell, J.A., Gogineni, S.P., Howat, I., Mouginot, J., Paden, J., Palmer, S., Rignot, E., and Steinhage, D.: A new bed elevation dataset for Greenland, The Cryosphere, 7, 499-510, https://doi.org/10.5194/tc-7-499-2013, 2013.

Benediktsson, Í., Aradóttir, N., Ingólfsson, Ó. and Brynjólfsson, S.: Cross-cutting palaeo-ice streams in NE-Iceland reveal shifting Iceland Ice Sheet dynamics, Geomorphology, 396, 1-16. https://doi.org/10.1016/j.geomorph.2021.108009, 2022.

Booth, D.B., and Hallet, B.: Channel networks carved by subglacial water: Observations and reconstruction in the eastern Puget Lowland of Washington, Geological Society of America Bulletin, 105, 671-683, 1993.

Booth, D.B., Troost, K.G., and Hagstrum, J.T.: Deformation of quaternary strata and its relationship to crustal folds and faults, south-central Puget Lowland, Washington State, Geology, 32:6, 505-508, https://doi.org/10.1130/G20355, 2004.

Clallam County, Olympic Department of Natural Resources, Washington Department of Transportation: Puget Lowlands 2005 [datafile]. Retrieved from https://lidarportal.dnr.wa.gov/#47.85003:-122.92053:7, 2008.

Clark, C.D.: Reconstructing the evolutionary dynamics of former ice sheets using multi-temporal evidence, remote sensing and GIS, Quaternary Science Reviews, 16:9, 1067-1092, https://doi.org/10.1016/S0277-3791(97)00037-1, 1997.

Clark, C.D.: Glaciodynamic context of subglacial bedform generation and preservation, Annals of Glaciology, 28, 23-32, https://doi.org/10.3189/172756499781821832, 1999.

Clark, C.D., Evans, D.J.A., and Piotrowski, J.A.: Palaeo-ice streams: an introduction, Boreas, 32:1, 1-3, https://doi.org/10.1080/03009480310001182, 2003.

Clark, C.D., Hughes, A.L.C., Greenwood, S.L., Spagnolo, M., and Ng, F.S.L.: Size and shape characteristics of drumlins, derived from a large sample, and associated scaling laws, Quaternary Science Reviews, 28:7-8, 677-696, https://doi.org/10.1016/j.quascirev.2008.08.035, 2009.

Cuffey, K.M., and Paterson, W.S.B.: The Physics of Glaciers: Fourth Edition, Academic Press, Burlington, Massachusetts, ISBN: 9780123694614, 2010.

Dethier, D.P., Pessl, F., Keuler, R.F., Balzarini, M.A., and Pevear, D.R.: Late Wisconsinan glaciomarine deposition and isostatic rebound, northern Puget Lowland, Washington, Geological Society of America Bulletin, 107:11, https://doi.org/10.1130/0016-7606(1995)1072.3.CO;2, 1995.

Durand, G., Gagliardini, O., Favier, L., Zwinger, T., and le Meur, E.: Impact of bedrock description on modeling ice sheet dynamics, Geophysical Research Letters, 38:20, https://doi.org/10.1029/2011GL048892, 2011.

Ehlers, J., Gibbard, P.L., and Hughes, P.D.: Quaternary Glaciations – Extent and Chronology, Elsevier, http://booksite.elsevier.com/9780444534477/index, 2010.

Eyles, N., Arbelaez Moreno, L., and Sookhan, S.: Ice streams of the Late Wisconsin Cordilleran Ice Sheet in western North America, Quaternary Science Reviews, 179, 87-122, https://doi.org/10.1016/j.quascirev.2017.10.027, 2018.

Eyles, N., and Doughty, M.: Glacially-streamlined hard and soft beds of the paleo-Ontario ice stream in Southern Ontario and New York state, Sedimentary Geology, 338, 51-71, https://doi.org/10.1016/j.sedgeo.2016.01.019, 2016.

Favier, L., Pattyn, F., Berger, S., and Drews, R.: Dynamic influence of pinning points on marine ice-sheet stability: a numerical study in Dronning Maud Land: East Antarctica, European Geosciences Union, 10:6, 2623-2635, https://doi.org/10.5194/tc-10-2623-2016, 2016.

Khazaradze, G., Qamar, A., and Dragert, H.: Tectonic deformation in western Washington from continuous GPS measurements, Geophysical Research Letters, 26:20, 3153-3156, https://doi.org/10.1029/1999GL010458, 1999.

King, E., Hindmarsh, R., and Stokes, C.: Formation of mega-scale glacial lineations observed beneath a West Antarctic ice stream, Nature Geoscience, 2 :8, 585-588, https://doi.org/10.1038/ngeo581, 2009.

Kleman, J., and Borgström, I.: Reconstruction of palaeo-ice sheets: The use of geomorphological data, Earth Surface Processes and landforms, 21:10, 893-909, https://doi.org/10.1002/(SICI)1096-9837(199610)21:103.0.CO;2-U, 1996.

Kleman, J., Hättestrand, C., Stroeven, A.P., Jansson, K.N., Angelis, H.D. and Borgström, I.: Reconstruction of Palaeo-Ice Sheets- Inversion of their Glacial Geomorphological Record, Glacier Science and Environmental Change, 192-198, https://doi.org/10.1002/9780470750636.ch38, 2006.

Kovanen, D.J., and Slaymaker, O.: Relict Shorelines and Ice Flow Patterns of the Northern Puget Lowland from Lidar Data and Digital Terrain Modelling, Geografiska Annaler, Series A, Physical Geography, 86:4, 385-400, jstor.org/stable/3566155, 2004.

Krabbendam, M., Eyles, N., Putkinen, N., Bradwell, T., and Arbelaez-Moreno, L.: Streamlined hard beds formed by palaeo ice stream: a review, Sedimentary Geology, 338, 24-50, https://doi.org/10.1016/j.sedgeo.2015.12.007, 2016.

MacKie, E. J., Schroeder, D. M., Caers, J., Siegfried, M. R., and Scheidt, C.: Antarctic topographic realizations and geostatistical modeling used to map subglacial lakes, Journal of Geophysical Research: Earth Surface, 125:3, https://doi.org/10.1029/2019JF005420, 2020.

MacKie, E.J., Schroeder, D.M., Zuo, C., Yin, Z., and Caers, J.: Stochastic modeling of subglacial topography exposes uncertainty in water routing at Jakobshavn Glacier, Journal of Glaciology, 67:261, 75-83, https://doi.org/10.1017/jog.2020.84, 2021.

McIntyre, N.F.: The Dynamics of Ice-Sheet Outlets: Journal of Glaciology, 31:108, 99-107. https://doi.org/10.1017/S0022143000006328, 1985.

McKenzie, M.A., Simkins, L.M., Principato, S., and Munevar-Garcia, S.: Subglacial bedform sensitivity to bed characteristics across the deglaciated Northern Hemisphere, Earth Surface Processes and Landforms, 47:9, 2341-2356, https://doi.org/10.1002/esp.5382, 2022.

McKenzie, M.A., Simkins, L.M., Slawson, J.S., and Wang, S.: Streamlined subglacial bedforms across isolated topographic highs in the Puget Lowland, Washington state, PANGAEA [data set], https://doi.org/10.1594/PANGAEA.954529, 2023.

Morlighem, M., Rignot, E., Binder, T., Blankenship, D., Drews, R., Eagles, G., et al.: Deep glacial troughs and stabilizing ridges unveiled beneath the margins of the Antarctic ice sheet, Nature Geoscience, 13:2, 132– 137, https://doi.org/10.1038/s41561-019-0510-8, 2020.

OCM Partners: 2017 USGS Lidar: Olympic Peninsula, WA from 2010-06-15 to 2010-08-15, NOAA National Centers for Environmental Information [datafile], https://www.fisheried.noaa.gov/inport/item/59232, 2019a.

OCM Partners: 2019 WA DNR Lidar: San Juan County, WA from 2010-06-15 to 2010-08-15, NOAA National Centers for Environmental Information [datafile], https://www.fisheries.noaa.gov/inport/item/67199, 2019b.

Payne, A., and Dongelmans, P.: Self-organization in the thermomechanical flow of ice sheets, Journal of Geophysical Research B: Solid Earth, 102:6, 12219-12233, https://doi.org/10.1029/97JB00513, 1997.

Pohjola, V.A., and Hedfors, J.: Studying the effects of strain heating on glacial flow within outlet glaciers from the Heimefrontfjella Range, Dronning Maud Land, Antarctica, Annals of Glaciology, 37, 134-142, https://doi.org/10.3189/172756403781815843, 2003.

Principato, S., Moyer, A., Hampsch, A. and Ipsen, H.: Using GIS and streamlined landforms to interpret palaeo-ice flow in northern Iceland, Boreas, 45:3, 470– 482, https://doi.org/10.1111/bor.12164, 2016.

Quantum Spatial, Inc.: Western Washington 3DEP LiDAR, United States Geological Survey [datafile], https://gismaps.snoco.org/metadata/topography/Western_Washington_3DEP_Technical_Data_Report.pdf, 2017.

Quantum Spatial, Inc.: Olympic Peninsula , Washington 3DEP LiDAR, United States Geological Survey [datafile], https://coast.noaa.gov/htdata/lidar3_z/geoid18/data/9072/supplemental/Olympic_Peninsula_3DEP_Area_1_LiDAR_Technical_Data_Report_revised_110419.pdf, 2019.

Robel, A. A., Pegler, S. S., Catania, G., Felikson, D., and Simkins, L. M.: Ambiguous stability of glaciers at bed peaks, Journal of Glaciology, 1-8, https://doi.org/10.1017/jog.2022.31, 2022.

Schoof, C., and Clarke, G., 2008, A model for spiral flows in basal ice and the formation of subglacial flutes based on a Reiner-Rivlin rheology for glacial ice: Journal of Geophysical Research: Solid Earth, v. 113 no. 5, p. 1-12. https://doi.org/10.1029/2007JB004957

Shaw, J., Pugin, A., and Young, R.R.: A meltwater origin for Antarctic shelf bedforms with special attention to megalineations, Geomorphology, 102:3-4, 364-375, https://doi.org/10.1016/0037-0738(89)90114-0, 2008.

Spagnolo, M., Clark, C.D., Ely, J.C., Stokes, C.R., Anderson, J.B., Andreassen, K., … and King, E.C.: Size, shape and spatial arrangement of mega-scale glacial lineations from a large and diverse dataset, Earth Surface Processes and Landforms, 39:11, 1432-1448, https://doi.org/10.1002/esp.3532, 2014.

Spagnolo, M., Clark, C.D., and Hughes, A.L.C.: Drumlin relief, Geomorphology, 153-154, 179-191, https://doi.org/10.1016/j.geomorph.2012.02.023, 2012.

Wang, S., Wu, Q., and Ward, D.: Automated delineation and characterization of drumlins using a contour tree approach, Int J Appl Earth Obs Geoinformation, 62, 144-156, https://doi.org/10.1016/j.jag.2017.06.006, 2017.

Winsborrow, M.C.M., Clark, C.D., and Stokes, C.R.: What controls the location of ice streams?, Earth-Science Reviews, 103, 45-59, https://doi.org/10.1016/j.earscirev.2010.07.003, 2010b.

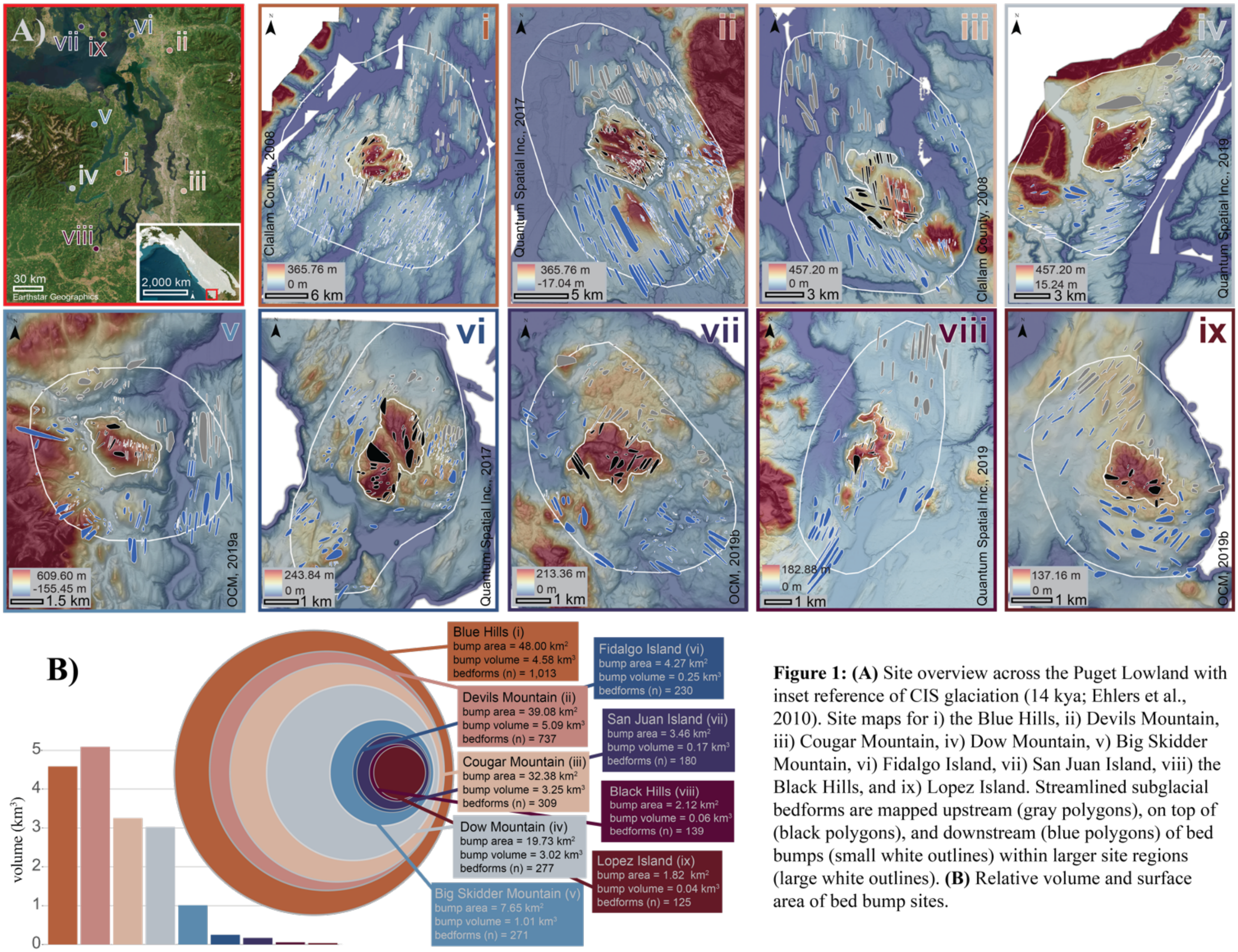

Figure 1. A) Site overview across the Puget Lowland with inset reference of CIS glaciation (14kya; Ehlers et al., 2010). Site maps for i) the Blue Hills, ii) Devils Mountain, iii) Cougar Mountain, iv) Dow Mountain, v) Big Skidder Mountain, vi) Fidalgo Island, vii) San Juan Island, viii) the Black Hills, and ix) Lopez Island. Streamlined subglacial bedforms are mapped upstream (gray polygons), on top of (black polygons), and downstream (blue polygons) of bed bumps (small white outlines) within larger site regions (large white outlines). B) Relative volume and surface area of bed bump sites.

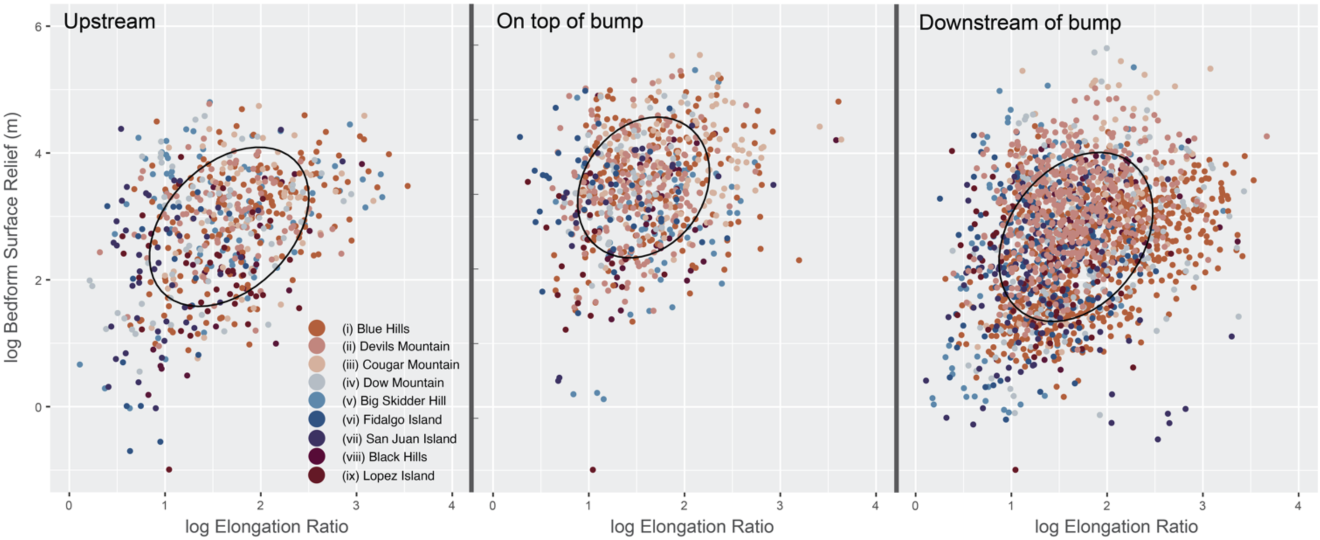

Figure 2: Scatterplots of the log of bedform elongation ratio and surface relief in meters. The ellipses are 1σ (68%) confidence levels for multivariate t-distributions for all bedforms (n=3,273). Sites are listed in the legend from largest surface area ((i) Blue Hills) to smallest surface area ((ix) Lopez Island).

Figure 2. Scatterplots of the log of bedform elongation ratio and surface relief in meters. The ellipses are 1σ (68%) confidence levels for multivariate t-distributions for all bedforms (n=3,273). Sites are listed in the legend from largest surface area ((i) Blue Hills) to smallest surface area ((ix) Lopez Island).

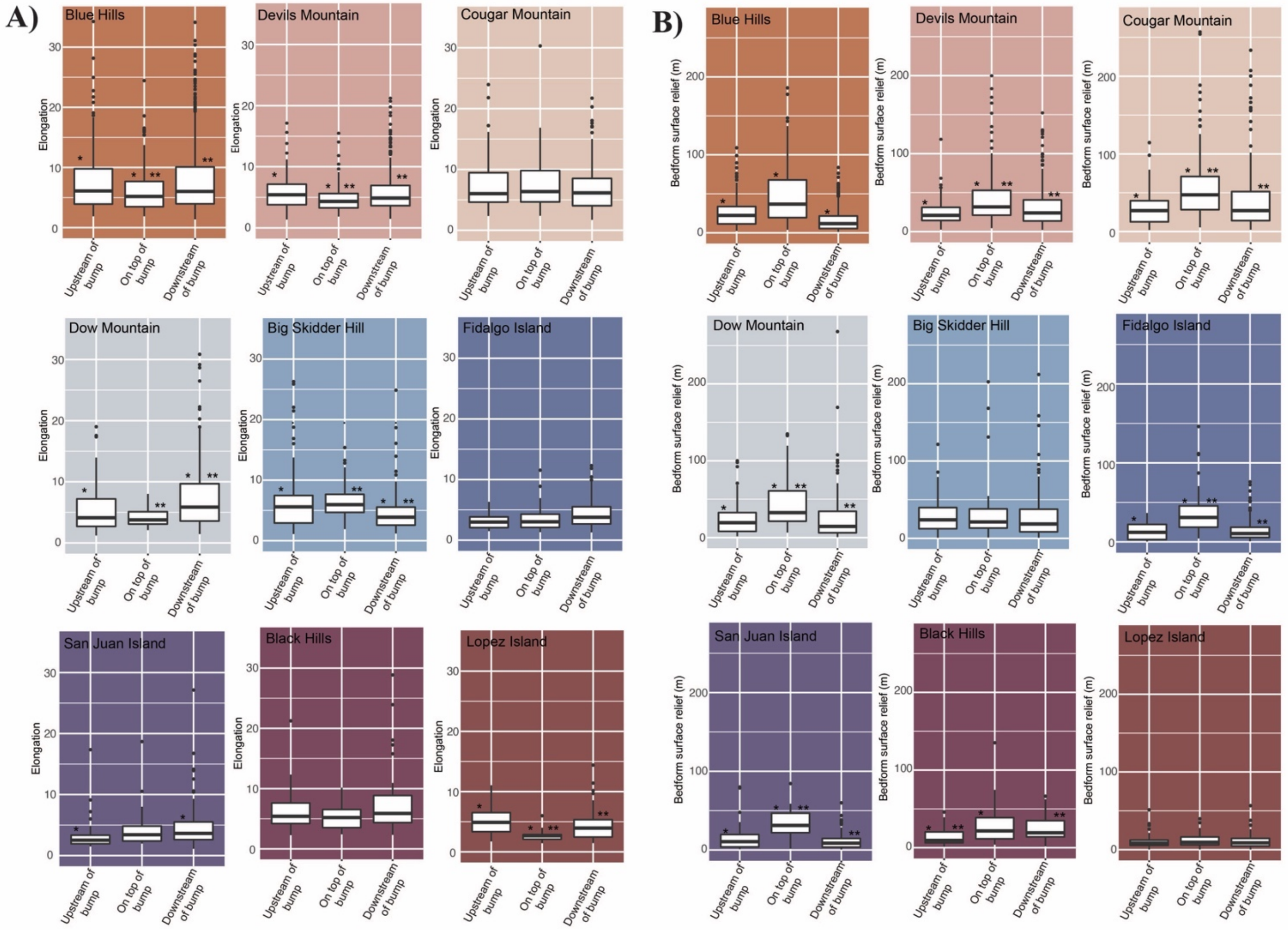

Figure 3: Box plots of A) bedform elongation data at each site with populations characterized upstream of, on top of, and downstream of bumps and B) bedform surface relief data at each site with populations characterized upstream of, on top of, and downstream of bumps. Statistically signficant differences between groups are indicated by asterisks. Multiple asterisks indicate a separate population with signficant differences, independent from other groups of statistical significance.

Figure 3. Box plots of A) bedform elongation data at each site with populations characterized upstream of, on top of, and downstream of bumps and B) surface relief data at each site with populations characterized upstream of, on top of, and downstream of bumps. Statistically significant differences between groups are indicated by asterisks. Multiple asterisks indicate a separate population with significant differences, independent from other groups of statistical significance.

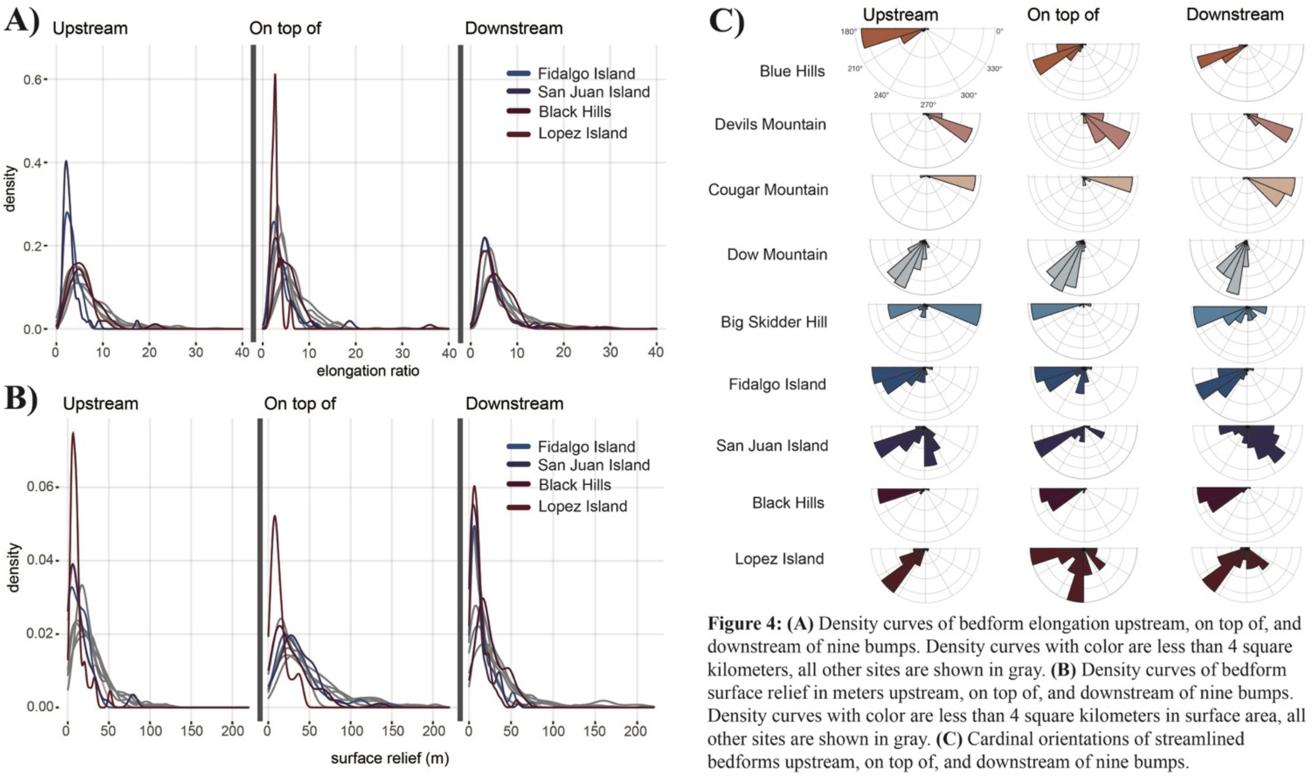

Figure 4: **(A)** Density curves of bedform elongation upstream, on top of, and downstream of nine bumps. Density curves with color are less than 4 square kilometers, all other sites are shown in gray. **(B)** Density curves of bedform surface relief in meters upstream, on top of, and downstream of nine bumps. Density curves with color are less than 4 square kilometers in surface area, all other sites are shown in gray. **(C)** Cardinal orientations of streamlined bedforms upstream, on top of, and downstream of nine bumps.

Figure 4. A) Density curves of bedform elongation upstream, on top of, and downstream of nine bumps. Density curves with color are less than 4 square kilometers, all other sites are shown in gray. B) Density curves of bedform surface relief in meters upstream, on top of, and downstream of nine bumps. Density curves with color are less than 4 square kilometers in surface area, all other sites are shown in gray. C) Cardinal orientations of streamlined bedforms upstream, on top of, and downstream of nine bumps.